The Astrophysical Journal Letters, 740:L15 (6pp), 2011 October 10 doi:10.1088/2041-8205/740/1/L15

GOODS-*HERSCHEL*: GAS-TO-DUST MASS RATIOS AND CO-TO-H_2 CONVERSION FACTORS IN NORMAL AND STARBURSTING GALAXIES AT HIGH-z

Georgios E. Magdis[1,2], E. Daddi[2], D. Elbaz[2], M. Sargent[2], M. Dickinson[3], H. Dannerbauer[2], H. Aussel[2], F. Walter[4], H. S. Hwang[2], V. Charmandaris[5,6,7], J. Hodge[4], D. Riechers[8], D. Rigopoulou[1], C. Carilli[9], M. Pannella[2], J. Mullaney[2], R. Leiton[2], and D. Scott[10]
[1] Department of Physics, University of Oxford, Keble Road, Oxford OX1 3RH, UK
[2] CEA, Laboratoire AIM, Irfu/SAp, F-91191 Gif-sur-Yvette, France
[3] NOAO, 950 N. Cherry Avenue, Tucson, AZ 85719, USA
[4] Max-Planck-Institut für Astronomie, Königstuhl 17, D-69117 Heidelberg, Germany
[5] Department of Physics & ICTP, University of Crete, GR-71003, Heraklion, Greece
[6] IESL/Foundation for Research & Technology-Hellas, GR-71110, Heraklion, Greece
[7] Chercheur Associé, Observatoire de Paris, F-75014, Paris, France
[8] Astronomy Department, California Institute of Technology, MC 249-17, 1200 East California Boulevard, Pasadena, CA 91125, USA
[9] National Radio Astronomy Observatory, P.O. Box O, Socorro, NM 87801, USA
[10] Department of Physics and Astronomy, University of British Columbia, Vancouver, BC V6T 1Z1, Canada
Received 2011 July 17; accepted 2011 August 26; published 2011 September 20

ABSTRACT

We explore the gas-to-dust mass ratio ($M_{\rm gas}/M_{\rm d}$) and the CO luminosity-to-$M_{\rm gas}$ conversion factor ($\alpha_{\rm CO}$) of two well-studied galaxies in the Great Observatories Origins Deep Survey North field that are expected to have different star-forming modes, the starburst GN20 at $z = 4.05$ and the normal star-forming galaxy BzK-21000 at $z = 1.52$. Detailed sampling is available for their Rayleigh–Jeans emission via ground-based millimeter (mm) interferometry (1.1–6.6 mm) along with *Herschel* PACS and SPIRE data that probe the peak of their infrared emission. Using the physically motivated Draine & Li models, as well as a modified blackbody function, we measure the dust mass ($M_{\rm dust}$) of the sources and find $(2.0^{+0.7}_{-0.6} \times 10^9)$ $M_\odot$ for GN20 and $(8.6^{+0.6}_{-0.9} \times 10^8)$ $M_\odot$ for BzK-21000. The addition of mm data reduces the uncertainties of the derived $M_{\rm dust}$ by a factor of $\sim$2, allowing the use of the local $M_{\rm gas}/M_{\rm d}$ versus metallicity relation to place constraints on the $\alpha_{\rm CO}$ values of the two sources. For GN20 we derive a conversion factor of $\alpha_{\rm CO} < 1.0$ $M_\odot$ pc^{-2} (K km s^{-1})$^{-1}$, consistent with that of local ultra-luminous infrared galaxies, while for BzK-21000 we find a considerably higher value, $\alpha_{\rm CO} \sim 4.0$ $M_\odot$ pc^{-2} (K km s^{-1})$^{-1}$, in agreement with an independent kinematic derivation reported previously. The implied star formation efficiency is $\sim$25 $L_\odot/M_\odot$ for BzK-21000, a factor of $\sim$5–10 lower than that of GN20. The findings for these two sources support the existence of different disk-like and starburst star formation modes in distant galaxies, although a larger sample is required to draw statistically robust results.

Key words: galaxies: evolution – galaxies: high-redshift – galaxies: starburst – galaxies: star formation – infrared: galaxies

Online-only material: color figures

1. INTRODUCTION

The determination of the conversion factor from CO luminosities to the molecular gas mass ($M_{\rm gas}$) of a galaxy ($\alpha_{\rm CO}$[11] $= M_{\rm gas}/L'_{\rm CO}$) remains an open issue as there is evidence that it varies considerably as a function of metallicity and intensity of the radiation field. Downes & Solomon (1998) showed that $\alpha_{\rm CO}$ is a factor of $\sim$6 smaller for local ultra-luminous infrared galaxies (ULIRGs; $L_{\rm IR} > 10^{12}$ $L_\odot$) than for local spiral galaxies. A similar picture seems to emerge at high redshift, with a fraction of submillimeter galaxies (SMGs) playing the role of local starbursts, having lower $\alpha_{\rm CO}$ values and exhibiting enhanced star formation efficiencies (defined as $L_{\rm IR}/M_{\rm gas}$), when compared to normal[12] star-forming galaxies selected by their rest-frame UV or optical light (Tacconi et al. 2008; Daddi et al. 2010a, 2010b; Genzel et al. 2010; Narayanan et al. 2011). Daddi et al. (2010a, 2010b) used a kinematic analysis of star-forming disk galaxies at $z \approx 1.5$ to argue that they have CO conversion factors $\alpha_{\rm CO} = 3.6 \pm 0.8$, similar to that in the Milky Way. Instead, Tacconi et al. (2008) and Carilli et al. (2010) placed an upper limit of $\sim$0.8 on the $\alpha_{\rm CO}$ value of high-z SMGs. Together with a variety of other evidence, these results support the existence of two distinct star formation regimes: a long-lasting mode for normal-disk galaxies and a more rapid mode for local starbursts and SMGs (Daddi et al. 2008, 2010a; Genzel et al. 2010). Nevertheless, excitation biases introduced by the use of different molecular lines, along with substantial uncertainties on the $\alpha_{\rm CO}$ values, raise potential concerns about the role of SMGs in this picture (e.g., Ivison et al. 2011).

Several studies in the local universe have tried to tackle this question by measuring the total dust mass of a galaxy ($M_{\rm dust}$) and assuming that it is proportional to $M_{\rm gas}$ (e.g., Leroy et al. 2011). However, determining $M_{\rm dust}$ is a complex task. In order to break degeneracies inherent in current models, a proper characterization of the peak of the spectral energy distribution (SED) of the source as well as of the Rayleigh–Jeans emission tail is required. With the wide wavelength coverage

[11] The units of $\alpha_{\rm CO}$, $M_\odot$ pc^{-2} (K km s^{-1})$^{-1}$, are omitted from the text for clarity.
[12] Throughout this Letter, we use the term "normal" to refer to star-forming galaxies that fall within the so-called main-sequence relation between their star formation rates and stellar masses (e.g., Brinchmann et al. 2004; Noeske et al. 2007; Elbaz et al. 2007, 2011; Magdis et al. 2010b). Instead, "starbursts" are galaxies with substantially elevated SFRs for their stellar masses.

(70–500 μm) of the *Herschel Space Observatory* (Pilbratt et al. 2010), we can now directly observe the peak of the IR emission of high-z galaxies. Together with ground-based millimeter (mm) observations that probe the Rayleigh–Jeans emission, this allows us to properly quantify $M_{\rm dust}$, and explore possible differences between the shape of the SEDs, the $M_{\rm gas}/M_{\rm d}$ ratios, and the $\alpha_{\rm CO}$ values of normal and starburst galaxies at high redshift.

As a test case, we combine *Herschel* PACS and SPIRE data, from the GOODS-*Herschel* program with (sub)mm observations for two of the best-studied high-z galaxies in the Great Observatories Origins Deep Survey North field (GOODS-N), the SMG GN20 at $z = 4.05$, and the normal star-forming galaxy, BzK-21000, at $z = 1.521$. The uniqueness of these sources relies on the detailed sampling of their Rayleigh–Jeans emission via ground-based mm interferometry (1.1–6.6 mm). Our aim is to derive $M_{\rm gas}/M_{\rm d}$ ratio estimates, investigate the slope of their SED in the Rayleigh–Jeans tail, and put constraints on the $\alpha_{\rm CO}$ values. Throughout this Letter we assume $\Omega_{\rm m} = 0.3$, $H_0 = 71$ km s^{-1} Mpc^{-1}, $\Omega_\Lambda = 0.7$, and Chabrier initial mass function.

2. SAMPLE AND OBSERVATIONS

We use deep 100 and 160 μm PACS and 250, 350, and 500 μm SPIRE observations of GOODS-N from the GOODS-H program. Details about the observations are given in Elbaz et al. (2011). *Herschel* fluxes are derived from point-spread function (PSF) fitting using *galfit* (Peng et al. 2002). A very extensive set of priors is used for 100, 160 and 250 μm, including all galaxies detected in the ultra-deep *Spitzer* Multiband Imaging Photometer (MIPS) 24 μm imaging, which effectively allow us to obtain robust flux estimates for relatively isolated sources, even beyond formal confusion limits at 250 μm. For 350 and 500 μm, this approach does not allow accurate measurements due to the increasingly large PSFs. Hence, we use a reduced set of priors based on Very Large Array (VLA) radio detections, resulting in flux uncertainties consistent with the confusion noise at these wavelengths. We note that in GN20, the radio priors also include the nearby GN20.2 objects (both"a" and "b" components; Daddi et al. 2009). A detailed description of the flux measurements and Monte Carlo (MC) derivations of the uncertainties will be presented elsewhere (E. Daddi et al. 2011, in preparation).

Originally detected at 850 μm by Pope et al. (2006), GN20 is one of the best-studied SMGs to date, the most luminous and also one of the most distant ($z = 4.055$; Daddi et al. 2009) in the GOODS-N field. It is detected in all *Herschel* bands apart from 100 μm. Carilli et al. (2010) reported the detection of the CO[1−0] and CO[2−1] lines with the VLA, and CO[6−5] and CO[5−4] lines with the Plateau de Bure Interferometer (PdBI) and the Combined Array for Research in Millimeter Astronomy (CARMA), respectively. The source is detected in the Aztec 1.1 mm map and continuum emission is also measured at 2.2, 3.3, and 6.6 mm (Carilli et al. 2011) and at 1.4 GHz with the VLA (Morrison et al. 2010). GN20 is identified in all Infrared Array Camera (IRAC) bands and at 24 μm while it appears as a *B*-band dropout in the Advanced Camera for Surveys-*Hubble Space Telescope* image. The stellar mass of the source is 2.3×10^{11} $M_\odot$ (Daddi et al. 2009). A compilation of the photometric data is given in Table 1.

BzK-21000 is a near-IR-selected star-forming galaxy, with a spectroscopic redshift, $z = 1.521$ (Daddi et al. 2008, 2010a). The source has secure detections in both PACS and in the first two SPIRE bands, while at 500 μm it is only marginally detected. In addition to IRAC and MIPS 24 μm data, the source is seen in the 16 μm InfraRed Spectrograph peak-up image (Teplitz et al. 2011). With follow-up VLA and PdBI observations, Dannerbauer et al. (2009), Aravena et al. (2010), and Daddi et al. (2008) have reported the detection of CO[3−2], CO[1−0], and CO[2−1] emission lines, respectively. Continuum detections and upper limits are also obtained at 1.1, 2.2, and 3.3 mm (Daddi et al. 2010a; Dannerbauer et al. 2009). The stellar mass is 7.8×10^{10} $M_\odot$ (Daddi et al. 2010a). The UV rest-frame morphology of this galaxy, the double-peaked CO profile, the large spatial extent of the CO reservoir, and the low gas excitation all provide strong evidence that this galaxy is a large, clumpy, rotating disk (Daddi et al. 2010a).

Table 1
Summary of *Herschel* and (sub)mm Data

λ (μm)	GN20 (mJy)	BzK-21000 (mJy)
100	0.7 ± 0.4[1]	8.1 ± 0.6[1]
160	5.4 ± 1.0[1]	15.1 ± 1.4[1]
250	18.6 ± 2.7[1]	24.4 ± 1.5[1]
350	41.3 ± 5.2[1]	20.1 ± 4.7[1]
500	39.7 ± 6.1[1]	11.6 ± 7.4[1]
850	20.3 ± 2.0[2]	...
1100	10.7 ± 1.0[3]	...
1300	...	0.87 ± 0.32[4]
2200	0.90 ± 0.15[5]	0.32 ± 0.15[6]
3300	0.33 ± 0.06[7]	0.04 ± 0.06[7]
6600	-0.01 ± 0.018[8]	...

References. (1) This Letter; (2) Pope et al. 2006; (3) Perera et al. 2008; (4) H. Dannerbauer et al. 2011, in preparation; (5) Dannerbauer et al. 2009; (6) Carilli et al. 2010; (7) Daddi et al. 2009; (8) Carilli et al. 2011.

3. ESTIMATING TOTAL DUST MASSES

We employ two methods to derive the dust mass of the galaxies: the physically motivated dust models of Draine & Li (2007, hereafter DL07), and a more simplistic, but widely used, modified blackbody model (MBB).

The DL07 models describe the interstellar dust as a mixture of carbonaceous grains and amorphous silicate grains. The properties of these grains are parameterized by the polycyclic aromatic hydrocarbon (PAH) index, $q_{\rm PAH}$, defined as the fraction of the dust mass in the form of PAH grains. The majority of the dust is supposed to be located in the diffuse interstellar medium (ISM), heated by a radiation field with a constant intensity $U_{\rm min}$. A smaller fraction γ of the dust is exposed to starlight with intensities ranging from $U_{\rm min}$ to $U_{\rm max}$, representing the dust enclosed in photodissociation regions. Following the prescription of DL07, we fit the rest-frame mid-IR to mm data points and search for the best-fit model by minimizing the reduced χ^2. The total dust mass is derived from the best-fit model and its uncertainty is estimated by the distribution of $M_{\rm d}$ values that correspond to models with $\chi^2 \leqslant \chi^2_{\rm min} + 1$ (Avni & Bahcall 1976). Although a different grain size distribution would result in different $M_{\rm dust}$, we choose to adopt the one prescribed by the DL07 models as they can successfully reproduce the IR and submillimeter emission for a sample of SINGS galaxies (including both normal and starburst galaxies).

We also fit the SEDs of our sources with the standard form of a single-temperature ($T_{\rm d}$) modified blackbody, leaving the effective emissivity ($\beta_{\rm eff}$) as a free parameter along with the

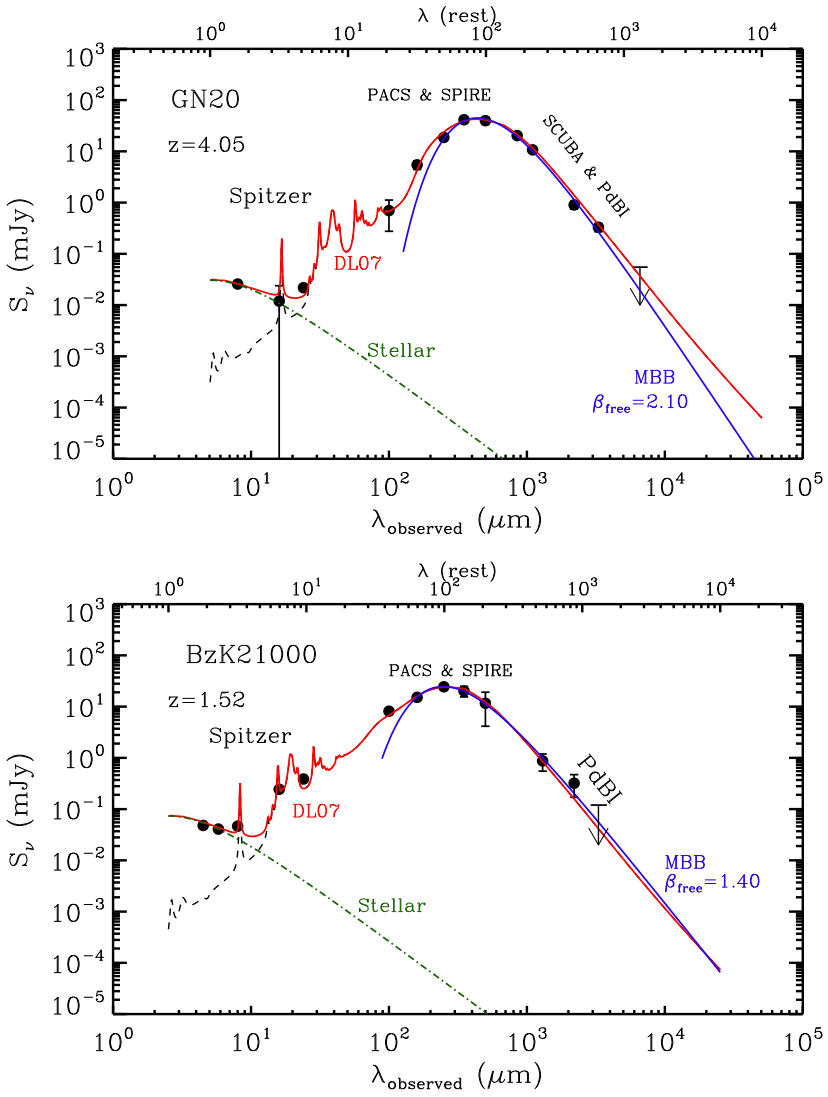

Figure 1. Observed SED of GN20 (top) and BzK-21000 (bottom) overlaid with the best-fit Draine & Li (2007, hereafter DL07) models (red) and the best-fit single-temperature modified blackbody (blue). The black dashed line is the DL07 model without the stellar component that is depicted with a green dotted-dashed line. The black arrows indicate the 3σ upper limit at 6.6 mm and 3.3 mm for GN20 and BzK-21000, respectively.

(A color version of this figure is available in the online journal.)

dust temperature (T_d). For the fit we only consider data points with $\lambda_{rest} > 40\,\mu$m, to avoid emission from very small grains and from the best-fit model we can then estimate the M_{dust} from the relation:

$$M_d = \frac{S_\nu D_L^2}{(1+z)\kappa_{rest} B_\nu(\lambda_{rest}, T_d)}, \quad (1)$$

where S_ν is the observed flux density, D_L is the luminosity distance, and $\kappa_{rest} = \kappa_0(\lambda_0/\lambda_{rest})^\beta$ is the rest-frame dust mass absorption coefficient at the observed wavelength (Li & Draine 2001). The uncertainty in M_{dust} is obtained as for the DL07 models. The photometric data along with the best-fitting DL07 and MBB models are shown in Figure 1, while in Table 2 we summarize the derived parameters.

The two methods return M_{dust} estimates that are in broad agreement. In particular, for GN20 we derive $M_{dust} = 2.0^{+0.7}_{-0.6} \times 10^9\ M_\odot$(DL07) and $1.5^{+0.4}_{-0.5} \times 10^9\ M_\odot$ (MBB) while for BzK-21000 the corresponding values are $M_{dust} = 8.6^{+0.6}_{-0.9} \times 10^8$ and $7.6^{+1.2}_{-1.3} \times 10^8\ M_\odot$. Best-fit MBB models also indicate $T_d = 33$ K and 34 K for GN20 and BzK-21000, respectively, and $\beta_{eff} = 2.1 \pm 0.2$ and 1.4 ± 0.2. The dependence of M_{dust} on the other two free parameters of the MBB models,[13] i.e., T_d and β_{eff}, along with the 68% and 99% confidence intervals, are shown in Figure 2.

To evaluate the significance of adding mm data in the derivation of M_{dust}, we repeat the fitting procedure, this time excluding any data at wavelengths longer than 850 μm. For the DL07 models, the best-fit M_{dust} are unaffected, but the uncertainties increase by a factor of ~2. Similar results are presented by several studies in the local universe (e.g., Draine et al. 2007; Galametz et al. 2011), where they find that in the absence of rest-frame (sub)mm data, the derived M_{dust} estimates are highly uncertain.

4. DISCUSSION

We derive a total IR luminosity of $L_{IR} = (1.9 \pm 0.4) \times 10^{13}\ L_\odot$ for GN20 and $L_{IR} = (2.1 \pm 0.3) \times 10^{12}\ L_\odot$ for BzK-21000 that

[13] These values are derived under the assumption of optical thinness. If we drop this assumption the corresponding values are $T_d = 33.8$ and 46.3 K for BzK2100 and GN20, respectively.

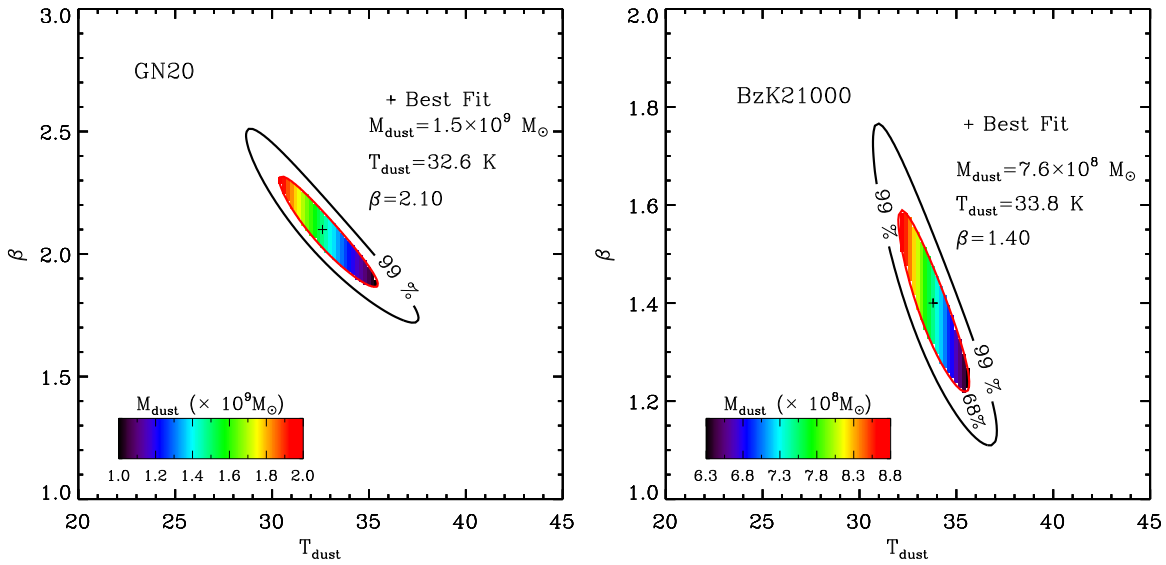

Figure 2. Uncertainties on the parameters derived by MBB models for the case of GN20 (left) and BzK-21000 (right). The plot shows the equivalent 68% and 99% confidence intervals on $\beta_{\rm eff}$ plotted against $T_{\rm d}$, as derived by MC simulations. The region enclosed by the 68% confidence level contour is color coded based on the $M_{\rm dust}$ that corresponds to each set of $\beta_{\rm eff}$ and $T_{\rm d}$. The best-fit value is denoted with a solid black cross (see also footnote 3).

(A color version of this figure is available in the online journal.)

Table 2
Summary of Derived Properties of GN20 and BzK-21000 with DL07 and MBB Models

Object	$L_{\rm IR}$ ($L_\odot$)	χ^2_ν (DL07)	$M_{\rm dust}$(DL07) ($10^8\ M_\odot$)	χ^2_ν (MBB)	$M_{\rm dust}$(MBB) ($10^8\ M_\odot$)	$T_{\rm d}$ (K)	β
GN20	$(1.9 \pm 0.4) \times 10^{13}$	2.14	21.0^{+7}_{-6}	1.54	15.0^{+6}_{-5}	32.6 ± 2.2	2.1 ± 0.2
BzK21	$(2.1 \pm 0.3) \times 10^{12}$	1.21	$8.6^{+0.6}_{-0.9}$	0.87	$7.6^{+1.2}_{-1.3}$	33.8 ± 2.1	1.4 ± 0.2

correspond to SFRs of ∼2000 and ∼210 $M_\odot$ yr^{-1} and specific star formation rates (sSFR) of ∼8.6 and ∼2.6 Gyr^{-1}. Several studies have shown that star-forming galaxies at any redshift follow a tight SFR–M_* relation, with outliers being starburst galaxies (e.g., Brinchmann et al. 2004; Elbaz et al. 2007; Daddi et al. 2007, 2009; Magdis et al. 2010a, 2010b). Our results confirm that the sSFR of BzK-21000 is similar to that of main-sequence galaxies defined in the SFR–M_* space at this redshift, while GN20 is located in the starburst regime.

As illustrated in Figure 1, it appears that GN20 has a steeper slope in the Rayleigh–Jeans tail when compared to that of BzK-21000. Despite the large uncertainties, the MBB analysis indicates that the $\beta_{\rm eff}$ values of two galaxies are different at a $\sim 2\sigma$ significance level. This difference in $\beta_{\rm eff}$ explains the similar effective $T_{\rm d}$ derived for the two sources despite the fact that the SED of GN20 peaks at ∼90 μm while that of BzK-21000 peaks at ∼100 μm. The best-fitting DL07 models suggest that BzK-21000 has properties similar to those found by Draine et al. (2007) for local spirals, with a larger fraction of dust in PAHs ($q_{\rm PAH} = 3.9\%$) and a less intense radiation field ($U_{\rm min} = 8$) compared to that in GN20 ($q_{\rm PAH} = 1.12\%$, $U_{\rm min} = 25$). Similar results are obtained by Elbaz et al. (2011).

Several studies have shown that there is a correlation between $M_{\rm gas}/M_{\rm d}$ and the enrichment of the ISM of a galaxy. In Figure 3 (left), we plot $M_{\rm gas}/M_{\rm d}$ versus metallicity for a local sample studied by Leroy et al. (2011). For consistency we have computed all metallicities on the Pettini & Pagel (2004, hereafter PP04) scale. This tight correlation (dispersion of ∼0.15 dex) can be used as a tool to constrain $\alpha_{\rm CO}$. In particular, if we know the metallicity of a galaxy and have measured its $M_{\rm dust}$, then we can estimate its $M_{\rm gas}$ and subsequently the $\alpha_{\rm CO}$ value of the source, if $L'_{\rm CO}$ is known. In what follows we will attempt to apply this approach to the two galaxies in our sample, under the assumption that the observed $M_{\rm gas}/M_{\rm d}$–metallicity relation for local galaxies holds at high redshift.

Having derived estimates for the $M_{\rm dust}$ values of our sources, we need information on their metallicities, for which we have to rely on indirect indicators. One of these is the M_*–metallicity relation of Erb et al. (2006), based on which BzK-21000 has a slightly sub-solar metallicity, $Z = 8.65$. A similar derivation would follow using the fundamental metallicity relation (FMR) of Mannucci et al. (2010) that relates the SFR and the stellar mass to metallicity.

For GN20, the situation is somewhat more complicated, as the Erb et al. (2006) relation is not sufficiently sampled at the high mass end ($>10^{11}\ M_\odot$). Using the FMR, and accounting for the evolution observed for galaxies at $z > 2.5$ (Mannucci et al. 2010), we derive a metallicity of $Z = 8.8$. Another metallicity estimate can be obtained by assuming that the huge SFR of GN20 could stem from the final burst of star formation, triggered by a major merger that will eventually transform the galaxy into a massive elliptical. Once star formation ceases, the mass and metallicity of the resulting galaxy will not change further, and one might therefore apply the mass–metallicity relation to present-day elliptical galaxies. In this scenario, the metallicity of GN20 could range between $Z = 8.8$ and 9.2, although a moderately super-solar metallicity is more probable. For our purposes we will adopt a metallicity of 8.65 ± 0.2 for BzK-21000 and a whole range of $Z = 8.8$–9.2 for GN20.

The fit to the local $M_{\rm gas}/M_{\rm d} - Z$ relation (Figure 3, left) indicates a value of $M_{\rm gas}/M_{\rm d} \sim 104$ for BzK-21000 and ∼75 (35) for GN20 assuming a metallicity of $Z = 8.8(9.2)$. Santini

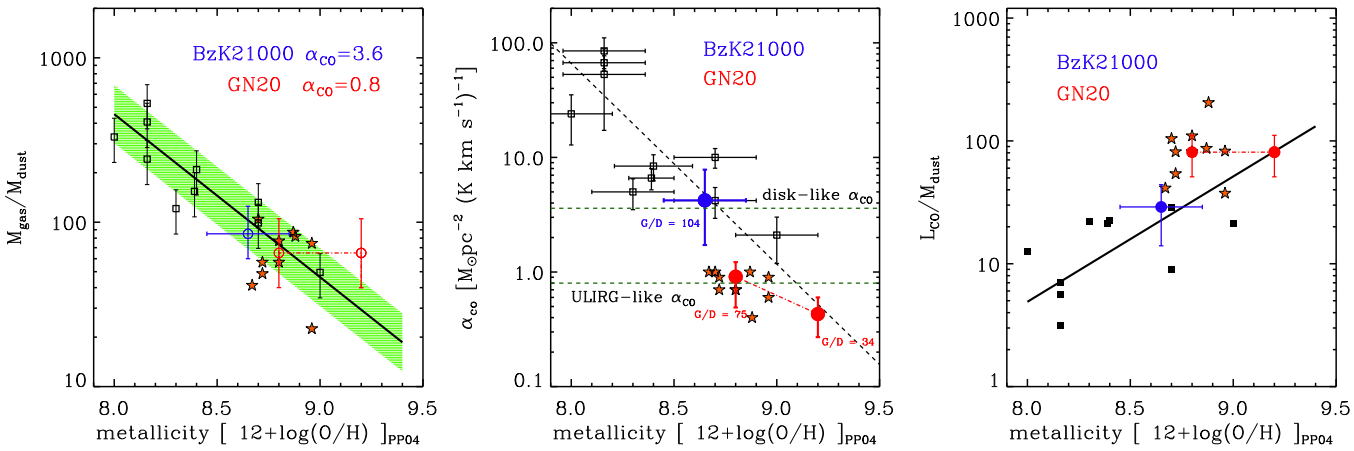

Figure 3. Left: M_{gas}/M_d vs. metallicity for a sample of galaxies in the Local Group by Leroy et al. (2011; black squares) and local ULIRGs by Solomon et al. (1997; orange stars). The solid black line the best linear regression fit to Leroy's sample and the green shadowed area depicts the dispersion of the correlation. Blue and red circles indicate the position of BzK-21000 and GN20, respectively, based on previously published M_{gas} values that correspond to $\alpha_{CO} = 3.6$ for BzK-21000 (Daddi et al. 2010a) and $\alpha_{CO} = 0.8$ for GN20 (Daddi et al. 2010a; Carilli et al. 2010). GN20 is placed at $Z = 8.8$ and $Z = 9.2$ which are the lower and upper limits for its metallicity. All metallicities are calculated on PP04 scale. Middle: constraints on α_{CO} based on the local M_{gas}/M_d–Z relation shown in the left panel. Colors and symbols are the same as in the left panel. Right: L'_{CO}/M_{dust} vs. metallicity for the same sample of galaxies.

(A color version of this figure is available in the online journal.)

et al. (2010) report similar $M_{gas}/M_d \sim 50$ for SMGs. Based on these ratios we first calculate M_{gas} for each galaxy and find $8.9\times10^{10}\ M_\odot$ and $1.5\times10^{11}\ M_\odot$ ($7.0\times10^{10}\ M_\odot$) for BzK-21000 and GN20, respectively. Then based on the relation $M_{gas} = \alpha_{CO} \times L'_{CO}$ we estimate the corresponding α_{CO} factors and find $\alpha_{CO} = 4.1^{+3.3}_{-2.7}$ for BzK-21000 and in the case of GN20 $\alpha_{CO} = 0.9^{+0.4}_{-0.5}$ for $Z = 8.8$ and $0.4^{+0.2}_{-0.2}$ for $Z = 9.2$. The derived values, along with the estimates of Leroy et al. (2011) for a local sample, are shown in Figure 3 (middle). We also overplot a sample of local ULIRGs from Solomon et al. (1997), for which we were able to compute their metallicities on the PP04 scale. The quoted uncertainties account both for the dispersion of the $M_{gas}/M_d - Z$ relation and the uncertainties in M_{gas}/M_d and M_{dust}.

The derived α_{CO} values agree with previous independent estimates. In particular, Daddi et al. (2010a), based on the dynamical masses of a sample of $z \sim 1.5$–2.0 BzK galaxies (including BzK-21000), argued for an average conversion factor of $\alpha_{CO} = 3.6$ for high-z star-forming disks and reported a value of $M_{gas} = (8.1 \pm 1.4) \times 10^{10}\ M_\odot$ for BzK-21000 (see also Aravena et al. 2010). Furthermore, Carilli et al. (2010), based on the CO[1 − 0] transition line, estimated the gas mass of GN20 to be $M_{gas} = 1.3 \times 10^{11} \times (\alpha_{CO}/0.8)\ M_\odot$, putting a coarse upper limit on the conversion factor of $\alpha_{CO} \sim 0.8$ from dynamical constraints. This indicates that our $\alpha_{CO} < 1.0$ estimate for GN20 is reasonable. Inverting this line of reasoning, placing the sources on the M_{gas}/M_d–metallicity plane of Figure 3 (left) based on the M_{gas} estimates from the literature, indicates that BzK-21000 is very close to the relation defined by a linear regression fit to the local sample. Similarly, GN20 appears to broadly follow the local trend. Another way to show that the M_{gas}/M_d–Z relation holds for high-z galaxies is to plot direct observables, without any assumptions for α_{CO}. Indeed, in Figure 3 (right), we plot L'_{CO}/M_{dust} versus metallicity for our sample and find again that both GN20 and BzK21000 follow the local trend. Finally, recent results from Genzel et al. (2011) seem to verify our assumption.

Despite the substantial uncertainties, the agreement with independent α_{CO} estimates is reassuring. In the local universe there is observational and theoretical evidence that α_{CO} in starburst galaxies is significantly smaller than that in the Milky Way disk (Downes & Solomon 1998; Scoville et al. 1997). The derived conversion factor for GN20 is consistent with that of local ULIRGs or even lower, while for BzK-21000 the value is considerably higher and close to that of local spirals. We stress that without the addition of the mm data, the large uncertainties in M_{dust} would not allow us to derive any meaningful conclusions. Furthermore, although the sources appear to have comparable $L_{IR}/L'_{CO} \sim 100\ L_\odot$ (K km s^{-1} pc^2)$^{-1}$, their star formation efficiencies (SFEs) are considerably different. In particular, for BzK-21000 we derive an SFE ∼25 while for GN20, SFE ∼100–200 (depending on the assumed metallicity). The two sources also have comparable $M_*/M_{dust} \sim 100$. This is also the case for local ULIRGs and normal Sloan Digital Sky Survey galaxies (da Cunha et al. 2010), supporting the idea that the property that distinguishes starbursts from normal star-forming galaxies is their enhanced SFR (at fixed M_{gas}, M_{dust}, and M_*).

We conclude by noting that our results, although limited to two sources, are in line with previous claims that the star formation mode of BzK-21000 and other high-z galaxies in the main sequence of the SFR–M_* plane is different from that of most SMGs, and more similar to that of local disks, despite their very large infrared luminosities and SFRs. Additionally, we confirm the validity of the widely adopted ULIRG-like α_{CO} factor for SMGs (e.g., Tacconi et al. 2008). We have also demonstrated that the combination of *Herschel* with ground-based mm data provides a powerful tool to investigate the dust and gas properties of high-z galaxies. A larger sample is needed to extend this investigation and draw statistically robust conclusions.

We thank Alvio Renzini for useful discussions. G.E.M. acknowledges support from Oxford University. E.D. acknowledges funding support from ERC-StG grant UPGAL 240039 and ANR-08-JCJC- 0008. D.R. acknowledges support from NASA through a *Spitzer Space Telescope* grant. This work is based on observations made with the *Herschel Space Observatory*, a European Space Agency Cornerstone Mission with significant participation by NASA.

REFERENCES

Aravena, M., Carilli, C., Daddi, E., et al. 2010, ApJ, 718, 177
Avni, Y., & Bahcall, N. A. 1976, ApJ, 209, 16
Brinchmann, J., Charlot, S., White, S. D. M., et al. 2004, MNRAS, 351, 1151
Carilli, C. L., Daddi, E., Riechers, D., et al. 2010, ApJ, 714, 1407
Carilli, C. L., Hodge, J., Walter, F., et al. 2011, ApJ, 739, L33
da Cunha, E., Charmandaris, V., Diaz-Santos, T., et al. 2010, A&A, 523, 78
Daddi, E., Bournaud, F., Walter, F., et al. 2010a, ApJ, 713, 686
Daddi, E., Dannerbauer, H., Elbaz, D., et al. 2008, ApJ, 673, 21
Daddi, E., Dannerbauer, H., Stern, D., et al. 2009, ApJ, 694, 1517
Daddi, E., Dickinson, M., Morrison, G., et al. 2007, ApJ, 670, 156
Daddi, E., Elbaz, D., Walter, F., et al. 2010b, ApJ, 714, 118
Dannerbauer, H., Daddi, E., Riechers, D. A., et al. 2009, ApJ, 698, 178
Downes, D., & Solomon, P. M. 1998, ApJ, 507, 615
Draine, B. T., Dale, D. A., Bendo, G., et al. 2007, ApJ, 663, 866
Draine, B. T., & Li, A. 2007, ApJ, 657, 810
Elbaz, D., Daddi, E., Le Borgne, D., et al. 2007, A&A, 468, 33
Elbaz, D., Dickinson, M., Hwang, H. S., et al. 2011, arXiv:1105.2537
Erb, D. K., Shapley, A. E., Pettini, M., et al. 2006, ApJ, 644, 813
Galametz, M., Madden, S. C., Galliano, F., et al. 2011, A&A, 532, 56
Genzel, R., Tacconi, L. J., Combes, F., et al. 2011, arXiv:1106.2098
Genzel, R., Tacconi, L. J., Gracia-Carpio, J., et al. 2010, MNRAS, 407, 2091
Ivison, R. J., Papadopoulos, P. P., Smail, I., et al. 2011, MNRAS, 412, 1913
Leroy, A. K., Bolatto, A., Gordon, K., et al. 2011, ApJ, 737, 12
Li, A., & Draine, B. T. 2001, ApJ, 554, 778
Magdis, G. E., Elbaz, D., Daddi, E., et al. 2010a, ApJ, 714, 1740
Magdis, G. E., Rigopoulou, D., Huang, J.-S., & Fazio, G. G. 2010b, MNRAS, 401, 1521
Mannucci, F., Cresci, G., Maiolino, R., Marconi, A., & Gnerucci, A. 2010, MNRAS, 408, 2115
Morrison, G. E., Owen, F. N., Dickinson, M., Ivison, R. J., & Ibar, E. 2010, ApJS, 188, 178
Narayanan, D., Krumholz, M., Ostriker, E. C., & Hernquist, L. 2011, arXiv:1104.4118
Noeske, K. G., Weiner, B. J., Faber, S. M., et al. 2007, ApJ, 660, 43
Peng, C. Y., Ho, L. C., Impey, C. D., & Rix, H-W. 2002, AJ, 124, 266
Perera, T. A., Chapin, E. L., Austermann, J. E., et al. 2008, MNRAS, 391, 1227
Pettini, M., & Pagel, B. E. J. 2004, MNRAS, 348, 59
Pilbratt, G. L., Riedinger, J. R., Passvogel, T., et al. 2010, A&A, 518, 1
Pope, A., Scott, D., Dickinson, M., et al. 2006, MNRAS, 370, 1185
Santini, P., Maiolino, R., Magnelli, B., et al. 2010, A&A, 518, 154
Scoville, N. Z., Yun, M. S., & Bryant, P. M. 1997, ApJ, 484, 702
Solomon, P. M., Downes, D., Radford, S. J. E., & Barrett, J. W. 1997, ApJ, 478, 144
Tacconi, L. J., Genzel, R., Smail, I., et al. 2008, ApJ, 680, 246
Teplitz, H. I., Chary, R.-R., Elbaz, D., et al. 2011, AJ, 141, 1